

Controlled Nanoscale Mechanical Phenomena Discovered with Ultrafast Electron Microscopy**

David J. Flannigan, Vladimir A. Lobastov, and Ahmed H. Zewail*

Dedicated to Professor Sir John Meurig Thomas on the occasion of his 75th birthday

For more than a century, the synthesis and control of nanoscale molecular structures has been at the forefront of many fields, such as organic/inorganic synthesis,^[1,2] chemical/biological catalysis,^[3,4] and crystallography.^[5] With light, especially with lasers, there exists another frontier in control whereby changes of population in or phases of the quantum states can be explored, and some intellectually interesting demonstrations have been reported.^[6] Recently, in the lexicon of nanoscience and nanotechnology, the interest has primarily focused on the development of nanoscale “devices” with functional purposes,^[7–10] such as the potential for nanoelectronics and possibly the making of mimics of biomachines, which operate with impressive molecular scale precision.^[11] Uncovering function of nanoscale phenomena requires direct imaging at sufficiently high spatial and temporal resolutions. As importantly, such visualization provides understanding of the fundamental nature of the physical forces, which derive the directed function in these complex systems.

Herein, we report the discovery of a mechanical nanoscale molecular phenomenon, a switchable channel or gate, observed with the newly developed ultrafast electron microscope, which is capable of imaging with the combined atomic-scale spatial and ultrafast temporal resolutions.^[12–16] The control is made using near infrared laser pulses, and the material is the crystalline quasi-one-dimensional semiconductor [Cu(TCNQ)] (TCNQ = 7,7,8,8-tetracyanoquinodimethane, C₁₂H₄N₄). Remarkably, the switching, after a shock, not only is reversible with the pulses being on or off, but also returns the material in space to the original structure. The functional behavior is robust in the relatively low-fluence regime. At significantly higher fluences, we observe, in the microscope, the internal dilation and the reduction of the copper ions to form islands of neutral copper metal structures. The power of ultrafast electron microscopy (UEM) is in the ability to visualize in situ these spatiotemporal behaviors, which are otherwise inferred from spectroscopic and post-event probing of films, as discussed below.

The strong electron acceptor (π acid) TCNQ undergoes a facile redox reaction at room temperature with metals such as silver and copper. In single crystals of the resulting [Cu(TCNQ)] charge-transfer complex, Cu⁺ and TCNQ^{•-} form discrete columnar stacks in a face-to-face configuration with strong overlap in the π system. Further, the copper atoms are bound in a four-coordinate highly distorted tetrahedral geometry to the nitrogen atoms on the cyano groups of the TCNQ molecules. The strong through-space interactions between the π electrons and the resulting quasi-one-dimensional structure of the material in the solid state impart interesting structural and electronic properties in the field of low-dimensional organic solids,^[17–19] and in the exploration of one-dimensional semiconducting nanostructures.^[20]

One property intrinsic to this material is the change in conductivity by the application of an external electric field. This change between two states has also been reported to occur by using light, and the effect was studied mainly by absorption and Raman spectroscopic probes.^[21–23] Photoablation of thin films was examined and shown, after ex situ radiation, to produce metal particles.^[24,25] Numerous reports have been made because of their unique properties, structure and synthesis,^[26–28] and potential applications as memory media.^[29–30] Intrinsic phenomena that arise solely from, for example, motion in space–time, could not be observed directly, thus leaving a whole parameter space unexplored in these and other materials.

For UEM studies of [Cu(TCNQ)], we examined single crystals (not films) synthesized directly on Si₃N₄ membrane grids by a solid/liquid reaction. Initial mapping of the sample by UEM showed that the synthetic methodology employed resulted in the growth of hundreds of [Cu(TCNQ)] crystalline rods ranging in width and length from several micrometers down to tens of nanometers. The crystallinity of the specimen was confirmed by selected-area electron diffraction in UEM, as shown below. [Cu(TCNQ)] is known to exist in both a kinetically favored state (phase I; needle crystal habit; Pn , $a = 3.8878$, $b = c = 11.266$ Å, $\alpha = \gamma = 90$, $\beta = 90.00(3)^\circ$) and a thermodynamically favored state (phase II; platelet crystal habit; $P2/n$, $a = 5.3337$, $b = 5.3312$, $c = 18.875$ Å, $\alpha = \gamma = 90$, $\beta = 94.036^\circ$).^[26] The material studied herein is that of phase I, as determined by the crystal habit and confirmed by indexing of the diffraction pattern. Importantly, during the initial characterization by UEM, no charging of the crystals was observed; no defocusing of the electron beam or motion of the specimen in the field of view was observed in all studies made. Details of the apparatus UEM1 can be found in references [13] and [16]. Herein, the excitation pulses were

[*] Dr. D. J. Flannigan, Dr. V. A. Lobastov, Prof. Dr. A. H. Zewail
Physical Biology Center for Ultrafast Science and Technology
California Institute of Technology
Pasadena, CA 91125 (USA)
Fax: (+1) 626-792-8456
E-mail: zewail@caltech.edu

[**] This work was supported by the Gordon and Betty Moore Foundation, the Air Force Office of Scientific Research, and the National Science Foundation. We wish to thank the referees for insightful comments.

used at 776 nm, whereas the electron pulses were generated by frequency doubling to provide the needed ultraviolet radiation. In the microscope, the two beams coincide spatially and temporally, and both real-space images and Fourier-space diffraction patterns were recorded and processed digitally. A mechanical shutter was placed in the excitation beam path to control a window of time when trains of optical pulses are on or off.

Figure 1 shows a [Cu(TCNQ)] single crystal that has been shocked by initially applying a burst of the laser light,

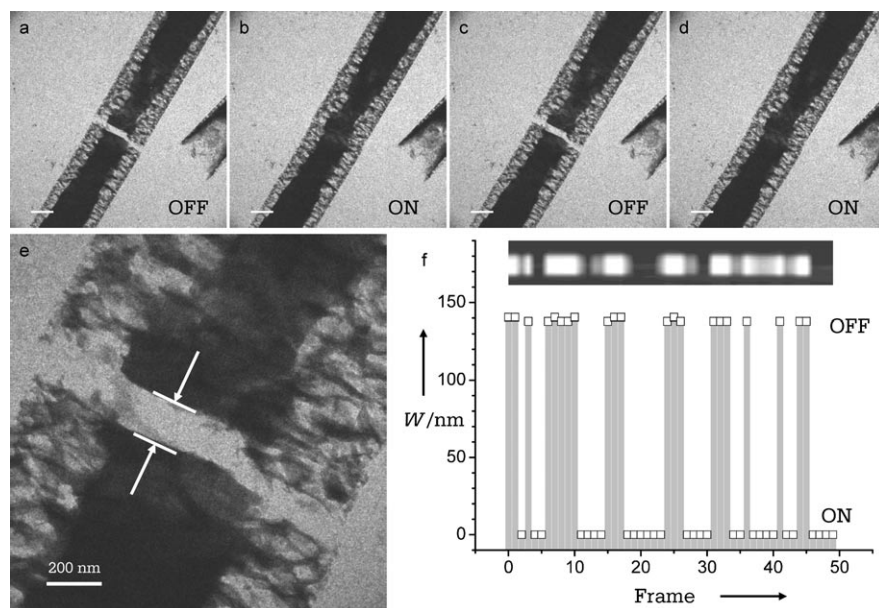


Figure 1. UEM images of channel gating: a–d) Sequential views (scale bar = 500 nm) of the already shocked [Cu(TCNQ)] single crystal in the “off” structure (a, c; no pulsed-laser irradiation) and in the “on” structure (b, d; pulsed-laser irradiation). e) Higher-resolution image of the crystal in the “off” structure illustrating the section within which quantification of the reproducibility of the expansion/contraction was performed. f) Plot showing the results of a sequence of “on” and “off” cycles. The channel width W varied from 0 (pulsed-laser irradiation) to 140 ± 5 nm (no pulsed-laser irradiation) over a series of 50 frames. The bar at the top is to illustrate the modulation in a memory recording. The difference in contrast along the edges is due to crystal shape and position on the substrate (crystal habit with thickness projected differently).

typically for $100 \mu\text{s}$ at a fluence of $0.5 \mu\text{J cm}^{-2}$ per pulse for 120-fs pulses with 80 MHz repetition rate. Following this shock, the crystal, which was micrometers in length, was directly observed in UEM1 to fracture and separate by tens of nanometers depending upon the fluence of the initial pulse sequence. When the shutter was open (i.e., the sample was irradiated with laser pulses) the crystal expanded along the long axis and closed the gap completely; that is, the two exposed faces of the crystal came into full contact. When the shutter was closed (i.e., the specimen was not irradiated with laser pulses) the material returned to its original structure in which the channel was again clearly observed. We then repeated these experiments by switching between the on and off modes. The crystal was observed to expand and contract along the long axis in synchrony with the shutter. However, the contrast of the image in the open zone changes to give a

relative value of 0.5 over the course of the recording time of 1 s, but the sharpness of the channel edges is maintained. From these experiments the timescale of the channel switching was estimated to be less than $10 \mu\text{s}$. The expansion/contraction was also observed in intact single crystals (i.e., not photoshocked) as changes at the ends of the material.

Four typical frames of the images obtained when the laser pulses are on or off are given in Figure 1 a–d. The higher-resolution image in Figure 1 e shows the nanoscale channel that is formed, in this case with a width of 140 nm. The

reversibility of gating is demonstrated in Figure 1 f by measuring the actual magnitude (distance) of the channel opening/closing while varying the number of frames recorded. For quantification of the data, we present in Figure 2 the diffraction patterns that were obtained in the microscope by the selected-area method, together with changes of the lattice spacing and channel width at different fluences. The diffraction pattern viewed along the [011] zone axis perpendicular to the stacking a axis ([100] direction) shows two distinct separations in Fourier space, S_{100} and S_{011} , whereby S is related to the corresponding planar spacing by the order of diffraction. Because the order is one, S and the interplanar distances are directly related. Thus, the values of 3.89 and 7.97 Å, respectively, were obtained for the distance between the planes, which agree well with those obtained by X-ray analysis of [Cu(TCNQ)] phase I.^[26]

The change in separation of these stacking planes (100) and those perpendicular (011) as a function of the energy deposited (fluence) is plotted in Figure 2 c, together with real-space values. For expansion along the a axis, the change is nearly linear until a relatively high fluence is reached, and

the rate of change is almost $1 \text{ \AA} \mu\text{J}^{-1} \text{ cm}^2$. For the perpendicular direction, there is no observable change within error. These “microscopic”, sub-angstrom, changes at the atomic scale were checked against the “macroscopic”, nanometer, channel formation. For comparison, the channel width as a function of fluence, shown in Figure 2 d, has a large rate of change of $220 \text{ nm} \mu\text{J}^{-1} \text{ cm}^2$. These results illustrate the significant change of the channel width with energy and the clear anisotropy along different directions, whereby the dominant change is along the stacking axis.

Conceptually, the macroscopic gating process can be understood from the microscopic structural dynamics. As seen in the crystal structure in Figure 3, the a axis is unique for stacking. Hence, the large anisotropy of gating must reflect the unique changes along the stacking axis [100] and not perpendicular to it. The modulation (i.e., closing and open-

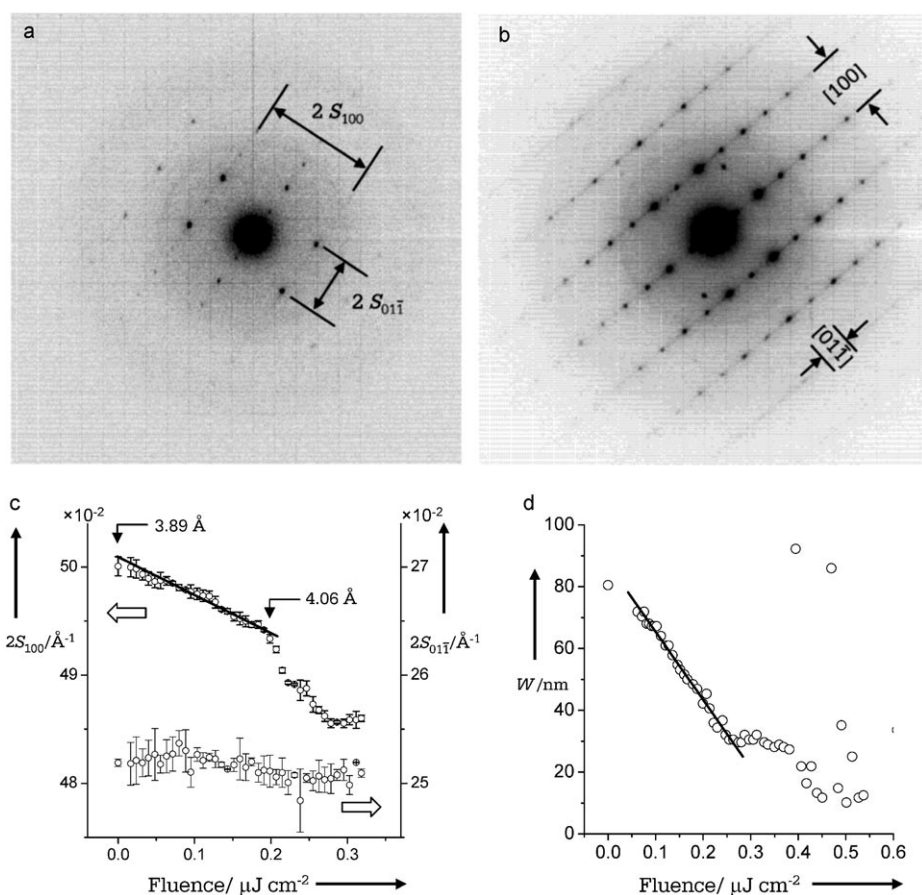


Figure 2. UEM diffraction patterns and effect of fluence on lattice spacings and channel width. Panels (a) and (c) illustrate the effects of increased laser fluence on the lattice structure of [Cu(TCNQ)] single crystals. The spacings in reciprocal space between the (100) and (011) planes were measured in the diffraction pattern (a) as a function of fluence and the results are plotted in (c). The real-space expansion that corresponds to the observed contraction in reciprocal space is labeled for two corresponding points in (c). b) Typical diffraction pattern obtained for a [Cu(TCNQ)] single crystal in UEM in which the electron beam is along the [011] zone axis. d) Plot of the channel width in real space as a function of laser fluence. The rates of expansion for each case are discussed in the text. Note the large anisotropy in the expansion along the stacking axis.

ing) of the channel is a modulation of the π -electron interactions of the stacked TCNQ molecules. Before exposure to laser pulses, the crystal is in the [Cu⁺TCNQ⁻] electronic structure. During the “on” period, the excitation creates a mixed-valence structure [Eq. (1)], as our crystals display absorption bands similar to the known charge-transfer band (600 to 1200 nm) in films.^[22,31] The mixed-valence structure leads to transport of charges and to a new lattice along the stacking direction.



The change in the a axis before melting of the crystal occurs calculated from the diffraction data in Figure 2 is approximately 0.2 Å. This change in intermolecular planes suggests that for a channel width of 40 nm, the macroscopic effective length over which the propagation is active should be around 2 μm (at 0.1 $\mu\text{J cm}^{-2}$ per pulse), which is indeed the

length scale of the material used. The agreement supports the notion that the macroscopic phenomenon is driven by the molecular interactions. The forward motion is not caused by equilibrium thermal heating because of the observed lack of expansion in the direction perpendicular to stacking (compare with Figure 2). Moreover, the thermal expansion coefficient for stacks of TCNQ molecules, although different by a factor of about 2 ($\alpha_{\text{stacking}} = 12 \times 10^{-5} \text{ K}^{-1}$; $\alpha_{\perp} = 5.8 \times 10^{-5} \text{ K}^{-1}$),^[32] predict a rise of at least 100 K at equilibrium, a rise which is not observed even when the pulse fluence is orders of magnitude larger than used here.^[33] It is possible, however, that a nonequilibrium heating on the nanoscale can drive the reversible change [see Eq. (1)].^[25]

In the linear regime of expansion, the channel width changes at the rate of 220 nm $\mu\text{J}^{-1} \text{ cm}^2$ in the crystals studied. The fluence varied from 0.05 to 0.60 $\mu\text{J cm}^{-2}$ per pulse at steps of 0.007 $\mu\text{J cm}^{-2}$, and the UEM image was acquired at each step. The gap spanning the two parts of the previously fractured crystal was quantified for each image at

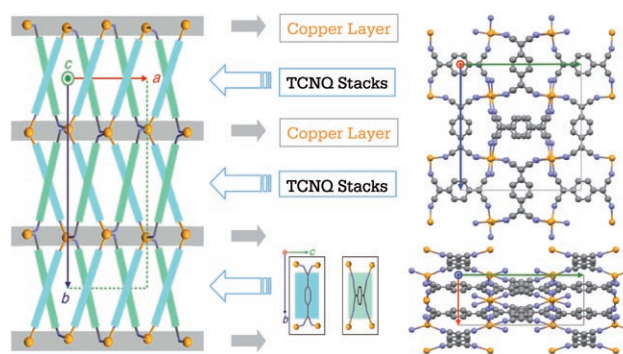


Figure 3. Conceptual representation of the molecular structure and the π stacking. The diagram on the left in conjunction with the diagrams of the single TCNQ molecules (lower center) illustrate how the molecules in neighboring stacks are rotated 90° from one another. The ball-and-stick diagram in the upper right of the figure illustrates this point further with a view of the crystal down the stacking a axis. The unit cell axes (a , b , c) are labeled in the diagram on the left, and the colors of the axes are carried over into the ball-and-stick diagrams on the right. The additional lines in the diagrams show the dimensions of the unit cell, which is essentially tetragonal. The stacked layered structure is responsible for the highly anisotropic properties of this material.

each laser fluence. It was found that the channel width decreased linearly as a function of fluence (i.e., the crystals expanded linearly along the *a* axis) up to $0.28 \mu\text{J cm}^{-2}$ per pulse, at which point the rate of crystal expansion became ill-defined owing to loss of crystallinity and formation of discrete domains corresponding to the individual atomic and molecular components of the material.

At higher fluences, the [Cu(TCNQ)] crystals were observed to lose all crystallinity and undergo a laser-induced reductive formation of copper metal domains along with strands of neutral TCNQ lying approximately perpendicular to the long axis of the crystal. It is interesting that even with UV excimer lasers, photoablation of polycrystalline films can produce metal particles.^[24] As shown in Figure 4, a single

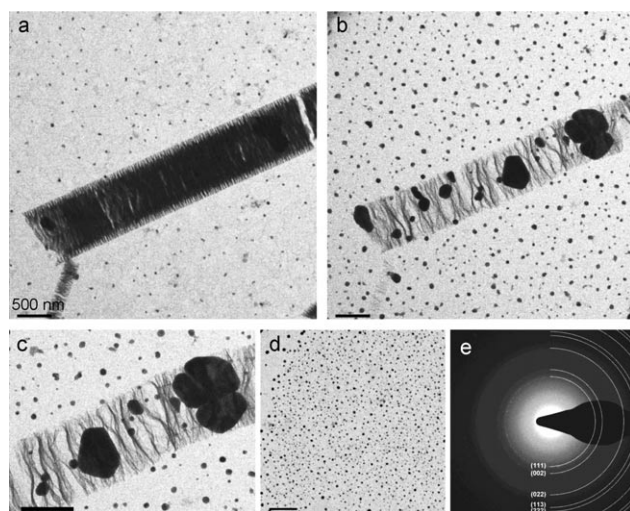


Figure 4. UEM images and diffraction at high fluences. a) A crystal of [Cu(TCNQ)] that has been irradiated at relatively low fluence. Some melting of the crystal is evident, although some order is still present. b) Nearly complete transformation of the [Cu(TCNQ)] crystal at high fluence showing discrete copper crystalline domains (c–e) along with strands that are likely charge-neutral TCNQ. The scale bar is the same in (a–d). e) Selected-area diffraction of the area in (c) shows the material to be crystalline copper metal. The diffraction is analyzed to show the characteristic pattern of copper metal.

crystal of [Cu(TCNQ)] can be exposed to laser pulses of increasing power, and when the fluence is high, isolated domains of copper metal are formed. Selected-area electron diffraction of these domains in UEM shows that they are composed of crystalline copper metal; thus the Cu^+ reduction process can be imaged at high fluences. In addition to these isolated copper metal domains, much smaller copper metal particles are also formed from a thin amorphous film of material, presumably [Cu(TCNQ)], underlying the single crystals (see selected area of the background in Figure 4d).

The controlling excitation at 1.6 eV is not only the key to gating of the channel at lower fluences, but also it is sufficient to facilitate charge transfer and hence weakening of copper bonding and enhancement of its mobility at higher fluences. The surface energy of metal clusters composed of a few atoms is quite large, and there is a strong driving force for the

smaller clusters to coalesce (Ostwald ripening). This behavior greatly enhances the formation of larger copper clusters and further reduces the ordered structure of the [Cu(TCNQ)] material until finally, at relatively high fluence, the crystal separates into its constituent atomic and molecular components. In the channel-gating regime, it is of interest to compare the threshold behavior at the fluences used here with those obtained using electric fields.^[22,25] At $0.1 \mu\text{J cm}^{-2}$ per pulse and using approximately 10^4 pulses in the window, the calculated electric field is about 10^3 V cm^{-1} , a value that is within an order of magnitude of that used with electric fields.^[22,25] We also note that previously reported damage of films with electrons^[25] did not occur in our UEM image and diffraction studies because of the very low number of electrons in each pulse.^[12–16] We see no deterioration of diffraction in UEM images, but it was severe when the microscope was operated in the conventional TEM mode with a thermally generated continuous beam.

Some final comments regarding the timescales involved: If the initial fracture, which results from the homogeneous illumination of the crystal, is driven by dislocations,^[34–36] it would occur at the speed of sound, which in this material is estimated to be 1.5 km s^{-1} , suggesting a timescale of 70 ps for the fracture to occur locally. However, if, under homogeneous illumination, fracture occurs by propagation in the material, the timescale would be nanoseconds. Similarly, if the speed of sound is the controlling velocity of the channel dynamics, then over a micrometer scale the time for closing and opening should be about one nanosecond. However, the charge transport in the mixed-valence state may in fact accelerate the process considerably. Knowing our fluence and the absorption cross section at the wavelength used, we estimate that the number of photons per copper atom is on the order of 10^{-5} , suggesting that the complete reduction of copper over the entire crystal will require about 10^5 of our pulses. Future experiments will utilize the excitation-probe scheme of UEM to resolve these different timescales.

In conclusion, it was possible to observe the reported phenomena of nanoscale structural changes because of the in situ capability of direct imaging and diffraction with UEM. Our initial interest in the TCNQ systems was to study the ultrafast dynamics, but in the process we realized a new dimension of UEM, namely, the study of macroscopic–microscopic transformations and the possible control with light or electrons of such transformations. The results discussed herein for channel formation and reductive metal clustering open the door to numerous further studies, including those of nucleation, charge/energy transport, and ultrafast dynamics of dislocations and coherent nuclear motions. The findings may be of value in applications involving molecular nanoswitches and channels, as well as optical pulse memory.

Received: September 8, 2007

Revised: October 8, 2007

Published online: November 6, 2007

Keywords: charge transfer · copper · electron diffraction · electron microscopy · quinodimethanes

- [1] E. J. Corey, *Angew. Chem.* **1991**, *103*, 469; *Angew. Chem. Int. Ed. Engl.* **1991**, *30*, 455.
- [2] J.-M. Lehn, *Angew. Chem.* **1988**, *100*, 91; *Angew. Chem. Int. Ed. Engl.* **1988**, *27*, 89.
- [3] J. M. Thomas, *Angew. Chem.* **1994**, *106*, 963; *Angew. Chem. Int. Ed. Engl.* **1994**, *33*, 913.
- [4] R. A. Lerner, S. J. Benkovic, P. G. Schultz, *Science* **1991**, *252*, 659.
- [5] A. H. Zewail, *The Chemical Bond: Structure and Dynamics*, Academic Press, Boston, **1992**.
- [6] *Femtochemistry VII: Fundamental Ultrafast Processes in Chemistry, Physics, and Biology* (Eds.: A. W. Castleman, Jr., M. L. Kimble), Boston, Elsevier, **2006**.
- [7] J. C. Love, L. A. Estroff, J. K. Kriebel, R. G. Nuzzo, G. M. Whitesides, *Chem. Rev.* **2005**, *105*, 1103.
- [8] A. Nitzan, M. A. Ratner, *Science* **2003**, *300*, 1384.
- [9] W. Lu, C. M. Lieber, *J. Phys. D* **2006**, *39*, R387.
- [10] C. P. Collier, E. W. Wong, M. Belohradský, F. M. Raymo, J. F. Stoddart, P. J. Kuekes, R. S. Williams, J. R. Heath, *Science* **1999**, *285*, 391.
- [11] R. D. Kornberg, *Proc. Natl. Acad. Sci. USA* **2007**, *104*, 12955.
- [12] For recent review, see: A. H. Zewail, *Annu. Rev. Phys. Chem.* **2006**, *57*, 65 and references therein.
- [13] V. A. Lobastov, R. Srinivasan, A. H. Zewail, *Proc. Natl. Acad. Sci. USA* **2005**, *102*, 7069.
- [14] M. S. Grinolds, V. A. Lobastov, J. Weissenrieder, A. H. Zewail, *Proc. Natl. Acad. Sci. USA* **2006**, *103*, 18427.
- [15] H. S. Park, J. S. Baskin, O.-H. Kwon, A. H. Zewail, *Nano Lett.* **2007**, *7*, 2545.
- [16] V. A. Lobastov, J. Weissenrieder, J. Tang, A. H. Zewail, *Nano Lett.* **2007**, *7*, 2552.
- [17] R. H. Friend, R. W. Gymer, A. B. Holmes, J. H. Burroughes, R. N. Marks, C. Taliani, D. D. C. Bradley, D. A. Dos Santos, J. L. Brédas, M. Lögdlund, W. R. Salaneck, *Nature* **1999**, *397*, 121.
- [18] A. J. Heeger, *Angew. Chem.* **2001**, *113*, 2660; *Angew. Chem. Int. Ed.* **2001**, *40*, 2591.
- [19] *Organic Electronics and Optoelectronics* (Eds.: S. R. Forrest, M. E. Thompson), *Chem. Rev.* **2007**, *107*, 923–1386.
- [20] H. Dai, E. W. Wong, C. M. Lieber, *Science* **1996**, *272*, 523.
- [21] E. I. Kamitsos, W. M. Risen, Jr., *Solid State Comm.* **1983**, *45*, 165.
- [22] E. I. Kamitsos, W. M. Risen, Jr., *J. Chem. Phys.* **1983**, *79*, 5808.
- [23] R. S. Potember, T. O. Poehler, R. C. Benson, *Appl. Phys. Lett.* **1982**, *41*, 548.
- [24] E. I. Kamitsos, A. C. Cefalas, S. Spyrou, C. A. Nicolaidis, *Synth. Met.* **1988**, *27*, 581.
- [25] E. I. Kamitsos, W. M. Risen, Jr., *Mol. Cryst. Liq. Cryst.* **1986**, *134*, 31.
- [26] R. A. Heintz, H. Zhao, X. Ouyang, G. Grandinetti, J. Cowen, K. R. Dunbar, *Inorg. Chem.* **1999**, *38*, 144.
- [27] K. Xiao, J. Tao, Z. Pan, A. A. Puzosky, I. N. Ivanov, S. J. Pennycook, D. B. Geohegan, *Angew. Chem.* **2007**, *119*, 2704; *Angew. Chem. Int. Ed.* **2007**, *46*, 2650.
- [28] Z. Zhou, K. Xiao, R. Jin, D. Mandrus, J. Tao, D. B. Geohegan, S. Pennycook, *Appl. Phys. Lett.* **2007**, *90*, 193115.
- [29] A. Graja, *Low-Dimensional Organic Conductors*, World Scientific, River Edge, **1992**.
- [30] *Lower-Dimensional Systems and Molecular Electronics* (Eds.: R. M. Metzger, P. Day, G. C. Papavassiliou), Plenum, New York, **1990**.
- [31] T. Oyamada, H. Tanaka, K. Matsushige, H. Sasabe, C. Adachi, *Appl. Phys. Lett.* **2003**, *83*, 1252.
- [32] S. van Smaalen, J. L. de Boer, C. Haas, J. Kommandeur, *Phys. Rev. B* **1985**, *31*, 3496.
- [33] P. Baum, D.-S. Yang, A. H. Zewail, *Science* **2007**, *318*, 788.
- [34] K. D. M. Harris, J. M. Thomas, *Cryst. Growth Des.* **2005**, *5*, 2124.
- [35] J. O. Williams, J. M. Thomas, *Mol. Cryst. Liq. Cryst.* **1972**, *16*, 223.
- [36] P. Hirsch, A. Howie, R. B. Nicholson, D. W. Pashley, M. J. Whelan, *Electron Microscopy of Thin Crystals*, Krieger Publishing, Malabar, **1977**.